Radio-frequency dielectric-barrier glow discharges in atmospheric argon

J. J. Shi and M. G. Kong[a)]
Department of Electronic and Electrical Engineering, Loughborough University, Loughborough, Leicestershire LE11 3TU, United Kingdom

(Received 28 November 2006; accepted 3 February 2007; published online 15 March 2007)

In this letter, an experimental investigation is presented to characterize the properties and benefits of radio-frequency (rf) dielectric-barrier discharges (DBDs) in atmospheric argon. Compared to rf atmospheric glow discharges generated with bare electrodes, atmospheric argon rf DBDs are shown to remain stable and uniform over a large current range from the α and the γ modes. Optical emission spectroscopy is used to show an active underpinning plasma chemistry and a gas temperature range of 461–562 K. These highlight the advantages of argon rf DBD as a surface processing technique over more expensive helium-based rf atmospheric glow discharges. © *2007 American Institute of Physics*. [DOI: 10.1063/1.2713141]

Atmospheric pressure glow discharges (APGDs) represent one of the most exciting topics in low-temperature plasma physics because of their potentially profound application impact, similar to that of low-pressure glow discharges in the semiconductor industry.[1] Free from the constraints of a vacuum chamber, APGD can be used to modify surface properties and functions over five orders of magnitude from 10 μm (Ref. 2) to a few meters.[3] This versatility has found APGD a very wide range of applications such as nanoscience,[4] biological decontamination,[5,6] plasma display,[2] and space exploration.[7] The majority of such applications has so far been achieved using a helium-dominant gas as the working gas, as this allows for an effective control of the glow-to-arc transition common in atmospheric discharges. It is, however, economically desirable to realize APGD applications with cheaper gases such as argon and nitrogen.[8] Using radio-frequency (rf) excitation with which gas breakdown voltage is low[9] and plasma stability is robust,[10] stable operation of Ar APGD has been reported usually as a jetlike plume suited for small-area processing applications.[11–13] Large-area Ar rf APGDs are much more difficult to achieve with the usual planar configuration of two parallel-plate bare electrodes,[14] and the few successful cases reported so far employ almost exclusively unconventional configurations.[15–17] In this letter, we report an experimental study of large-area Ar rf atmospheric glow discharges sustained between two parallel dielectrically insulated electrodes. The objectives of the work are to study (a) an alternative of producing large-area rf APGD in argon and (b) the generic characteristics of Ar rf APGDs in a simple electrode configuration that may be applicable to other electrode configurations.[11–17]

The argon rf atmospheric discharge considered in this study was generated between two parallel stainless-steel plates each covered with a ceramic sheet of 0.5 mm in thickness and 9.0 in relative permittivity. Its electrode unit was enclosed in a Perspex box with an argon flow of 5 SLM (standard liters per minute) at 760 torr. This is essentially a rf dielectric-barrier discharge (DBD) in atmospheric argon, and its characteristics in atmospheric helium have been studied both theoretically[18] and experimentally.[19] To distinguish it from conventional atmospheric discharges generated between two bare electrodes, the latter is referred to as rf APGD. The diameter of the electrodes was 20 mm, and the gas gap was fixed at 2.0 mm. To produce a comparable rf APGD, the same electrode unit was employed without the ceramic sheets and with the gas gap fixed at 2.0 mm. For both the rf DBD and the rf APGD, one electrode was powered, via a homemade impedance matching network, by a radio-frequency power source system, in which a 13.56 MHz sinusoidal signal was generated by a function generator and then amplified by a power amplifier (AR 150A100B). The discharge current and the applied voltage were measured by a wideband current probe (Tektronix P6021) and a wideband voltage probe (Tektronix P6015A), and their wave forms were recorded on a digital oscilloscope. With the triggering signal provided by a pulse generator, an intensified charge coupled device (iCCD) camera (Andor i-Star DH720) was used to capture the plasma images with 1 ns exposure time. Optical emission spectrum was obtained using a spectrometer system with a focal length of 0.3 m and a grating of 600 or 2400 grooves/mm.

Figure 1 shows typical voltage and current traces of the rf DBD. The gas voltage was obtained as the difference between the applied voltage and the memory voltage across the dielectric barriers, the latter of which was measured through the discharge current.[8] For all plasma conditions considered,

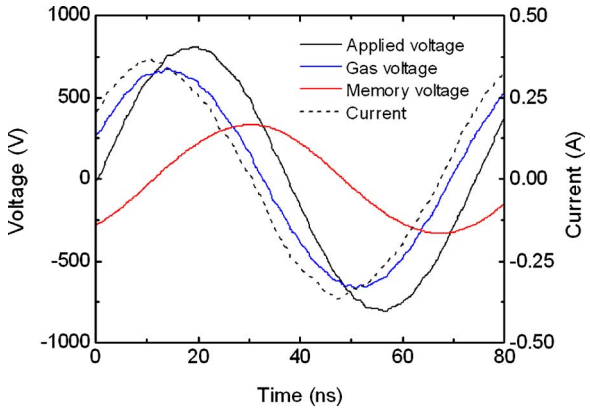

FIG. 1. (Color online) Typical traces of the discharge current, the applied and the gas gap voltages, and the memory voltage across the dielectric barriers for an argon rf DBD.

[a)]Author to whom correspondence should be addressed; electronic mail: m.g.kong@lboro.ac.uk

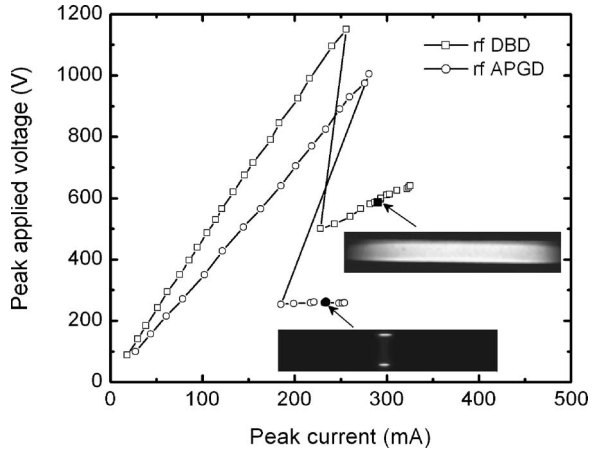

FIG. 2. Current dependence of the applied voltage in the argon rf DBD and the rf APGD. Inserts are the images of the large-area rf DBD and the constricted rf APGD at 285.0 and 260.5 mA, respectively.

both the applied and the gas voltages were found to be sinusoidal. This is different from kilohertz homogeneous DBD of which the gas voltage has a pulselike waveform.[8] The discharge current of the rf DBD has a smooth and largely sinusoidal wave form, free from any spikes and very different from that of kilohertz DBDs which typically have a spiky current waveform.[8] The smooth wave form of the discharge current and the gas voltage suggest that the argon rf DBD is unlikely to be filamentary. For both the Ar rf DBD and Ar rf APGD, the current is seen in Fig. 2 to have an initially linear relationship with the applied voltage. Both straight lines go through the origin, and they represent the prebreakdown regime for the two discharges. The slope of the rf DBD is greater than that of the rf APGD, since the total impedance in the rf DBD electrode unit is larger with the dielectric layers in the absence of the discharge. Gas breakdown occurred at a peak applied voltage of 1150 V in the rf DBD and at 1005 V in the rf APGD. The larger breakdown voltage in the rf DBD was due to the addition of the two ceramic sheets that divided into the applied voltage.

At gas breakdown, both atmospheric argon discharges underwent a large voltage drop not seen in rf atmospheric helium discharges.[18,19] The peak applied voltage of the argon rf DBD reduced by 650 V from V_p=1150 to 500 V, whereas that of the argon rf APGD decreased by 752 V from 1005 to 253 V. If the input rf power was increased further immediately after gas breakdown, the resulting rf APGD usually took the form of a *constricted* plasma column as shown in the bottom insert in Fig. 2. This constricted plasma was imaged at a peak discharge current of I_p=260.5 mA using the iCCD camera with 1 ms exposure time. It is seen in Fig. 2 to have a diameter of approximately 1 mm and was found to move around between the two bare electrodes. From an application standpoint, this rf APGD in Fig. 2 is of little use. By contrast, the introduction of the two ceramic sheets was found to produce large-area atmospheric argon discharge as illustrated by the inserted plasma image for the rf DBD. Taken at I_p=285.0 mA and again with the iCCD camera, the rf DBD is seen to cover the entire electrode surface uniformly and fill up the entire space between the two electrodes. The rf DBD was found to be stable up to I_p=324 mA, which reached the output limit of the power amplifier.

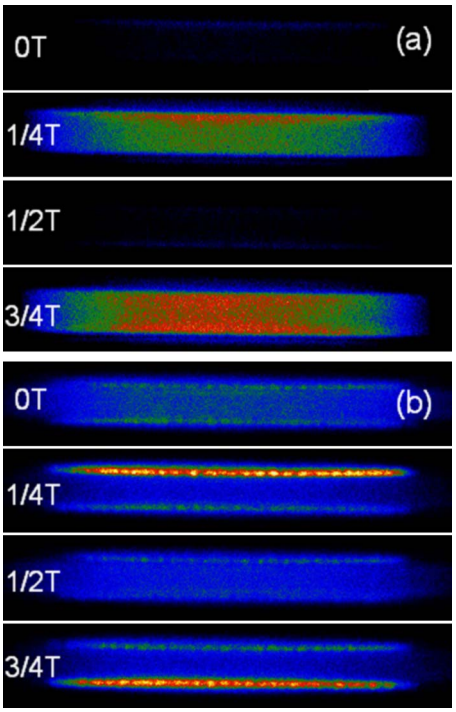

FIG. 3. (Color online) 1 ns and single-exposure images of the Ar rf DBD at four equally spaced instants at (a) 228 mA and (b) 311 mA.

Figure 3 show single-shot images of the argon rf DBD with 1 ns exposure time and without image summation. The absence of streamers from the single-exposure plasma images provides the most direct evidence of the spatial uniformity of the argon rf DBD. With four sequential plasma images taken at of I_p=228.0 mA and at t=0, $T/4$, $T/2$, and $3T/4$ with T being the rf period, Fig. 3(a) shows a volumetric appearance of a large-area and streamer-free rf DBD in atmospheric argon with a periodically varying optical emission intensity. This stable and large-area atmospheric argon discharge is much more desirable for applications than the constricted Ar rf APGD in Fig. 2. Also significant is the observation that the Ar rf DBD in Fig. 3(a) does not appear to have an apparent negative glow. This would suggest an α mode.[20,21] In Fig. 3(b) for which four images of the Ar rf DBD were taken at a peak current of 311 mA, their spatial uniformity and the periodic variation in the optical intensity are similar to those in Fig. 3(a). One significant difference is, however, the clear appearance of the negative glow, suggesting a full establishment of the sheath region and its alternative appearance near the instantaneous cathode through one rf cycle.[22,23] These are typical of a γ mode.[20,21] Therefore, the evolution of the Ar rf DBD from immediately after gas breakdown to the last point of 324 mA in Fig. 2 was accompanied by a mode transition from the volumetric α mode to the sheath-dominant γ mode. In helium rf APGD, this mode transition is often related to the change of the differential conductivity from being positive to negative.[22,24] Yet, the differential conductivity of the Ar rf DBD in Fig. 2 remains positive even though its images in Fig. 3 suggests a mode transition. This is due to the voltage shown in Fig. 2 being the applied voltage rather than the gap voltage.

Optical emission spectrum was also measured for the Ar rf DBD, as shown in Fig. 4 at I_p=311 mA. Nitrogen lines are apparent in the 300–550 nm range, whereas the atomic oxygen lines at 777 and 844 nm are also seen in Fig. 4(a). The

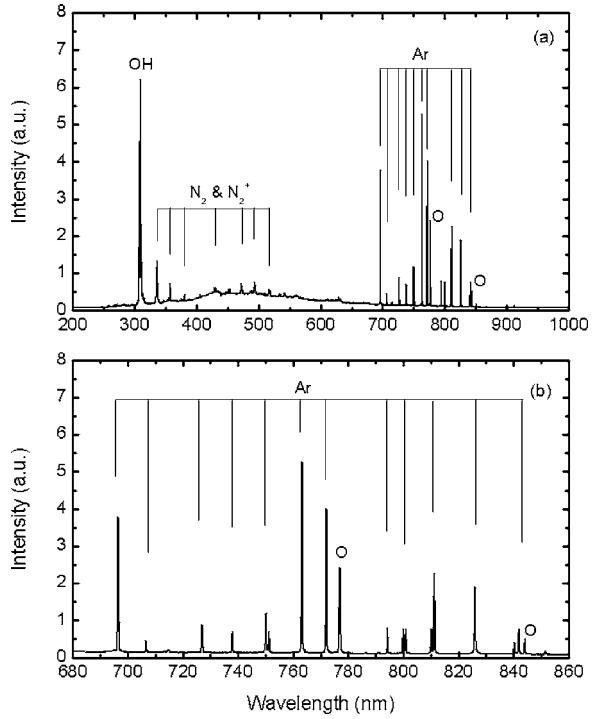

FIG. 4. Optical emission spectrum of the argon rf DBD at I_p=311 mA.

appearance of the nitrogen and oxygen lines is a result of the plasma-enclosing Perspex box not being airtight and the impurity gases in the industrial grade argon gas. The OH line at 309 nm is also significant. The spectral band from 700 to 850 nm is dominated by strong argon lines at 697, 707, 727, 738, 751, 763, 772, 795, 801, 811, 826, 841, and 843 nm, of which the line intensities at 697, 763, and 772 nm are the strongest. Compared to rf APGD jets,[12] the argon lines in rf DBD are more numerous and indicative of an active underpinning plasma chemistry. For example, optical emission at 763, 801, 826, 841, and 843 nm was found to be weak in an Ar rf APGD jet.[12] Also in an Ar rf atmospheric plasma generated with multiple ground electrodes,[16] the 772 nm line was found to be not as strong as the 811 nm line, thus exhibiting an interesting contrast to the spectrum of Fig. 4(b).

With a grating of 2400 grooves/mm, optical emission spectrum was used to estimate the gas temperature. By comparing the shape of the measured OH line around 309 nm with LIFBASS simulation data,[25] the rotational temperature was obtained. As shown in Fig. 5 as a function of the peak discharge current, the gas temperature of the Ar rf DBD varies from 461 to 562 K, much higher than the gas temperature in helium rf DBD (Ref. 18 and 19) but similar to that in other Ar rf atmospheric plasma.[12,22] This temperature range is suitable for many surface modification applications.[1,16] It is also worth mentioning that the S-shape dependence of the gas temperature on the discharge current suggests a saturation of the temperature rise at large currents and so an intrinsic ability of the rf DBD to control thermal runaway.

In conclusion, it has been demonstrated that the introduction of dielectric barriers can critically enable the generation of large-area and stable rf glow discharges in atmospheric argon over a large range of the discharge current.

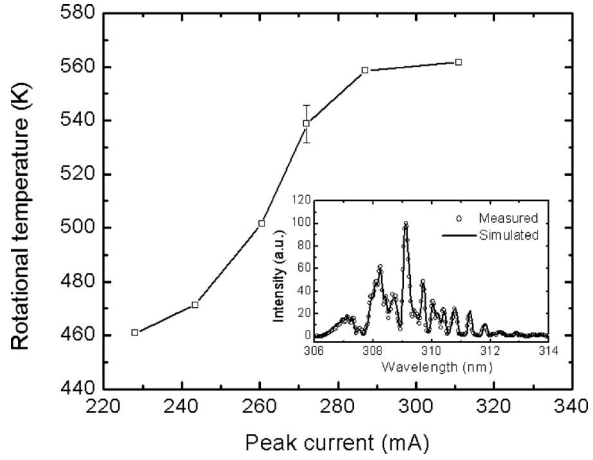

FIG. 5. Dependence of the gas temperature on the discharge current. The insert illustrates the comparison of the measured OH line at 309 nm with simulated data.

Nanosecond images have provided evidence of mode transition, and optical emission spectroscopy has indicated active underpinning plasma chemistry. Gas temperature has been found spectroscopically to be in the 461–562 K range, well suited for a wide range of surface processing applications.

This work was funded by the Department of Health, U.K.

[1]U. Kogelschatz, Plasma Chem. Plasma Process. **23**, 1 (2003).
[2]J. G. Eden and S. J. Park, Phys. Plasmas **13**, 057101 (2006).
[3]For the industrial scale, see for example, http://www.apjet.com/services.html#prodscale
[4]H. Shirai, T. Kobayashi, and Y. Hasegawa, Appl. Phys. Lett. **87**, 143112 (2005).
[5]M. Laroussi, IEEE Trans. Plasma Sci. **28**, 184 (2000).
[6]X. T. Deng, J. J. Shi, G. Shama, and M. G. Kong, Appl. Phys. Lett. **87**, 153901 (2005).
[7]Y. Takao and K. Ono, Plasma Sources Sci. Technol. **15**, 211 (2006).
[8]N. Gherardi and F. Massines, IEEE Trans. Plasma Sci. **29**, 536 (2001).
[9]J. Park, I. Henins, H. W. Herrmann, and G. S. Selwyn, J. Appl. Phys. **89**, 15 (2001).
[10]J. J. Shi and M. G. Kong, Appl. Phys. Lett. **87**, 201501 (2005).
[11]H. Yoshiki, A. Oki, H. Ogawa, and Y. Horiiki, Thin Solid Films **407**, 156 (2002).
[12]S. Wang, V. Schulz-von der Gathen, and H. F. Dobele, Appl. Phys. Lett. **83**, 3272 (2003).
[13]M. Moravej, X. Yang, R. F. Hicks, J. Penelon, and S. E. Babayan, J. Appl. Phys. **99**, 093305 (2006).
[14]H. B. Wang, W. T. Sun, H. P. Li, C. Y. Bao, X. Gao, and H. Y. Luo, Appl. Phys. Lett. **89**, 161504 (2006).
[15]K. H. Gericke, C. Gebner, and P. Scheffler, Vacuum **65**, 291 (2002).
[16]S. Y. Moon, J. W. Han, and W. Choe, Thin Solid Films **506-507**, 355 (2006).
[17]A. Rahman, A. P. Yalin, V. Surla, O. Stan, K. Hoshimiya, Z. Yu, E. Littlefield, and G. J. Collins, Plasma Sources Sci. Technol. **13**, 537 (2004).
[18]J. J. Shi, D. W. Liu, and M. G. Kong, Appl. Phys. Lett. **89**, 081502 (2006).
[19]J. J. Shi, D. W. Liu, and M. G. Kong, Appl. Phys. Lett. **90**, 031505 (2007).
[20]J. J. Shi and M. G. Kong, J. Appl. Phys. **97**, 023306 (2005).
[21]J. J. Shi and M. G. Kong, IEEE Trans. Plasma Sci. **33**, 624 (2005).
[22]S. Y. Moon, J. W. Han, and W. Choe, Phys. Plasmas **13**, 013504 (2006).
[23]J. J. Shi and M. G. Kong, Phys. Rev. Lett. **96**, 105009 (2006).
[24]J. J. Shi, X. T. Deng, R. Hall, J. D. Punnett, and M. G. Kong, J. Appl. Phys. **94**, 6303 (2003).
[25]J. Luque and D. R. Crosley, SRI International Report No. MP 99-009, 1999 (http://www.sri.com/psd/lifbase/).